Crystals 2020
The 2nd International Online Conference on Crystals
10–20 NOVEMBER 2020 | ONLINE
crystals MDPI

Lithium niobate: from single crystals to nanocrystals

László Kovács*, Laura Kocsor, Gabriella Dravecz, László Péter, Krisztián Lengyel, and Gábor Corradi

Wigner Research Centre for Physics, Konkoly-Thege M. út 29-33, 1121 Budapest, Hungary

* Corresponding author: kovacs.laszlo@wigner.hu

Abstract: $LiNbO_3$ single crystals were first grown more than 50 years ago. Since that time thousands of papers have been published dealing with their outstanding ferroelectric, acoustic, nonlinear optical, holographic etc. properties and demonstrating their countless realized or potential applications. It was about 25 years ago, when the first stoichiometric $LiNbO_3$ crystals gave a new impulse to the never-ending investigations. Different applications require different undoped or doped systems of bulk, thin film, or nanocrystal forms. In the present talk I'll show two examples, (i) incorporation of dopants into stoichiometric crystals, and (ii) properties of $LiNbO_3$ nanocrystals prepared by high-energy ball-milling.

Dopants are generally used to tailor the crystal properties for a given application. To understand the effect of dopants the substitution site in the crystal have to be known. Our IR absorption studies unambiguously showed that for the di-, tri-, and tetravalent cations a threshold concentration exists above which the dopants partially substitute at Nb sites, while below it they can be found on Li sites.

Nano-crystalline $LiNbO_3$ was prepared from single crystals by the high-energy ball-milling technique. During milling the material suffered partial reduction that lead to the formation of bipolarons and polarons yielding gray color together with Li_2O segregation on the open surfaces. Upon high temperature oxidation a $LiNb_3O_8$ shell was formed. The particle size of the nano-crystals were determined by dynamic light scattering (DLS) and scanning electron microscopic (SEM) methods.

Keywords: lithium niobate; single crystal; nanocrystal;

OUTLINE

i) Dopant sites in stoichiometric $LiNbO_3$ single crystals

- Stoichiometric vs. congruent $LiNbO_3$ (SLN ↔ CLN)
- Hydroxyl ions in SLN
- Optical damage resistant (ODR) ions
- Rare-earth (RE) ions
- Transition metal (TM) ions (Fe^{3+}, Cr^{3+}, Ti^{4+})

ii) Mechanochemical reactions of $LiNbO_3$ induced by high-energy ball-milling

- Lithium niobate nanocrystals
- High-energy ball-milling (dry and wet grinding)
- Particle and grain size reduction
- Phase transformation and chemical reaction
- Structure characterization (X-ray, Raman, reflection spectroscopy, coulometric titration, electron microscopy)

i) Stoichiometric vs. congruent $LiNbO_3$

Phase diagram, crystal growth

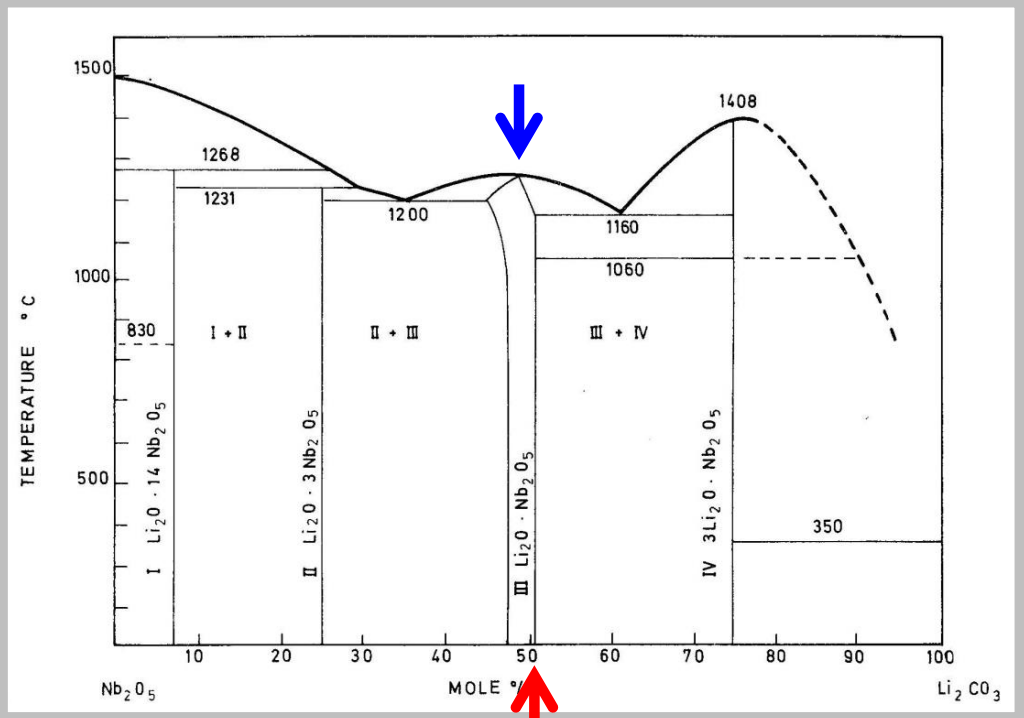

$LiNbO_3$ melts congruently
grown by the Czochralski method

48.4 mol% Li_2O
51.6 mol% Nb_2O_5
Li/Nb ≈ 0.94
$Li_{1-5z}Nb_{1+z}O_3$ ($z \approx 0.01$)

Stoichiometric crystals
grown by the HTTSSG method
from K_2O flux

K/Nb = 0.31, Li/Nb = 1 in the flux
K ≈ 0, Li/Nb ≈ 1 in the crystal
$LiNbO_3$ ($z \approx 0$)

K. Polgár, Á. Péter, L. Kovács, G. Corradi, Zs. Szaller: Growth of stoichiometric $LiNbO_3$ single crystals by top seeded solution growth method, *Journal of Crystal Growth*, **177**, 211-216, 1997.

Crystals 2020

i) Stoichiometric vs. congruent $LiNbO_3$

OH^- absorption band

OH^- ions are probes of the defect structure in $LiNbO_3$

Congruent (Li/Nb ≈ 0.94)
$Li_{1-5z}Nb_{1+z}O_3$ ($z \approx 0.01$)
$\nu_{max} \approx 3484\ cm^{-1}$

Stoichiometric (Li/Nb ≈ 1)
$LiNbO_3$ ($z \approx 0$)
$\nu_{max} = 3466\ cm^{-1}$

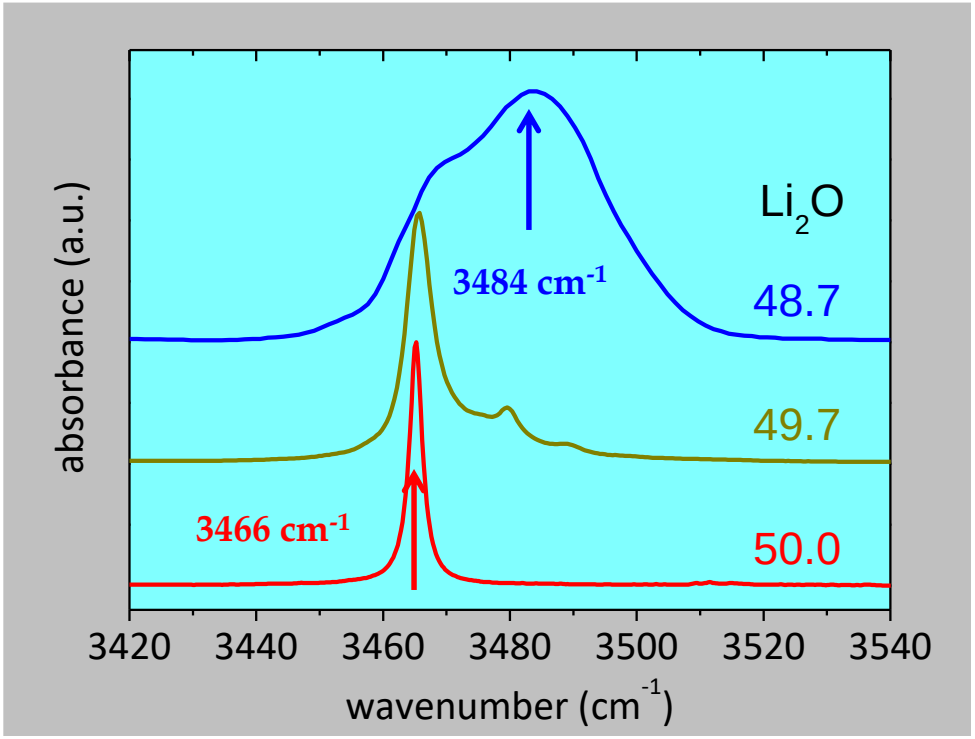

Stretching vibration of OH^- ions in $LiNbO_3$

K. Polgár, Á. Péter, L. Kovács, G. Corradi, Zs. Szaller: Growth of stoichiometric $LiNbO_3$ single crystals by top seeded solution growth method, *Journal of Crystal Growth*, **177**, 211-216, 1997.

Crystals 2020

i) Dopant ions in $LiNbO_3$

- Transition metal (TM) ions: **$Fe^{2+/3+}$, Mn^{2+}, $Cu^{+/2+}$, Ni^{2+}, Cr^{3+}, Ti^{4+}, etc.**
  - Increase the photorefractive sensitivity utilized in holographic recording
  - Surface layer diffused Ti^{4+} is used in optical waveguides
- Optical damage resistant (ODR) ions: **Mg^{2+}, Zn^{2+}, Sc^{3+}, In^{3+}, Hf^{4+}, Zr^{4+}, Sn^{4+}**
  - ODR ions above a **threshold concentration** suppress the photorefractive damage
  - The threshold concentration depends on the valence state of the dopant and the composition of LN (much lower for stoichiometric LN).
- Rare earth ions: **Pr^{3+}, Nd^{3+}, Dy^{3+}, Er^{3+}, Yb^{3+}, …**
  - Laser active dopants, 4f - 4f transitions
  - Quantum Information Processing (QIP), Quantum Optics

i) Threshold concentration of ODR dopants

Below threshold $M^{n+} \rightarrow Li^{+}$ for n = 2, 3, 4 reducing the number of Nb_{Li}

Above threshold $M^{n+} \rightarrow Li^{+}$ and Nb^{5+} no Nb_{Li} ions are left in the crystal

Congruent $LiNbO_3$ ($Li_{1-5z}Nb_{1+z}O_3$ ($z \approx 0.01$), $Nb_{Li} \approx 0.01$)

Stoichiometric $LiNbO_3$ ($Li_{1-5z}Nb_{1+z}O_3$ ($z \approx 0$), $Nb_{Li} \approx 0$)

No excess Nb – no Nb_{Li} $C_{th} \approx 0$ mol%

Experimentally – almost fulfilled

- for Mg^{2+} $C_{th} \approx 0.2$ mol% in sLN << $C_{th} \approx 5$ mol% in cLN
- for Zr^{4+} $C_{th} \approx 0.09$ mol% in sLN << $C_{th} \approx 2$ mol% in cLN

The OH^- absorption spectrum is one of the best indicator of the threshold effect

Á. Péter, K. Polgár, L. Kovács, K. Lengyel: Threshold concentration of MgO in near-stoichiometric $LiNbO_3$ crystals , *Journal of Crystal Growth*, **284**, 149-155, 2005.
L. Kovács, Zs. Szaller, K. Lengyel, Á. Péter, I. Hajdara, G. Mandula, L. Pálfalvi, J. Hebling: Photorefractive damage resistance threshold in stoichiometric $LiNbO_3$:Zr crystals, *Optics Letters*, **38**, 2861-2864, 2013.

i) Hydroxyl ions in ODR ion doped SLN

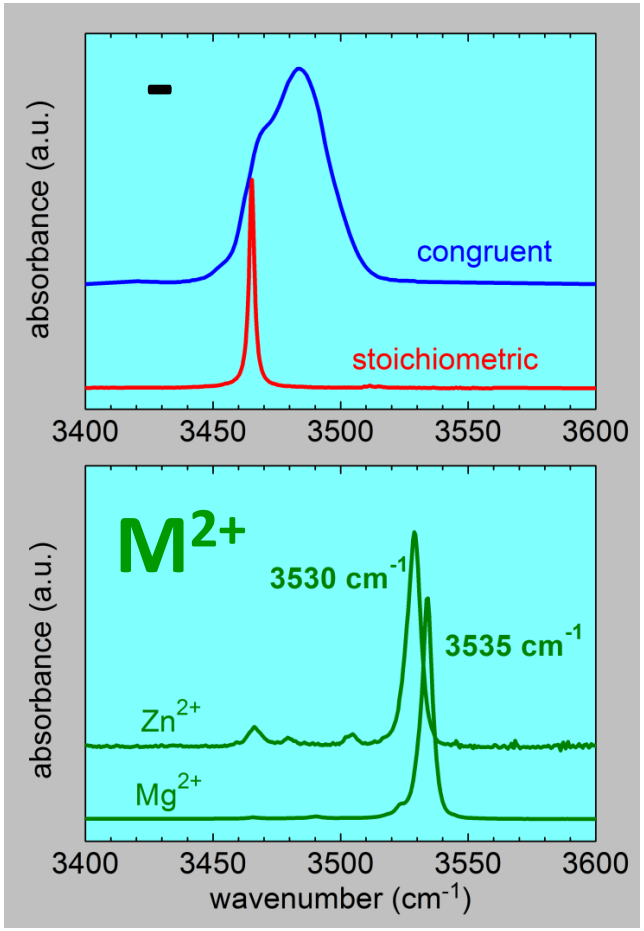

ODR ion	OH^- vibrational frequency (cm^{-1}) below — above threshold	
Mg^{2+}	3466	**3535**
Zn^{2+}	3466	**3530**
In^{3+}	3466	**3504**
Sc^{3+}	3466	**3505**
Hf^{4+}	3466	**3476**
Zr^{4+}	3466	**3475**
Sn^{4+}	3466	**3474**

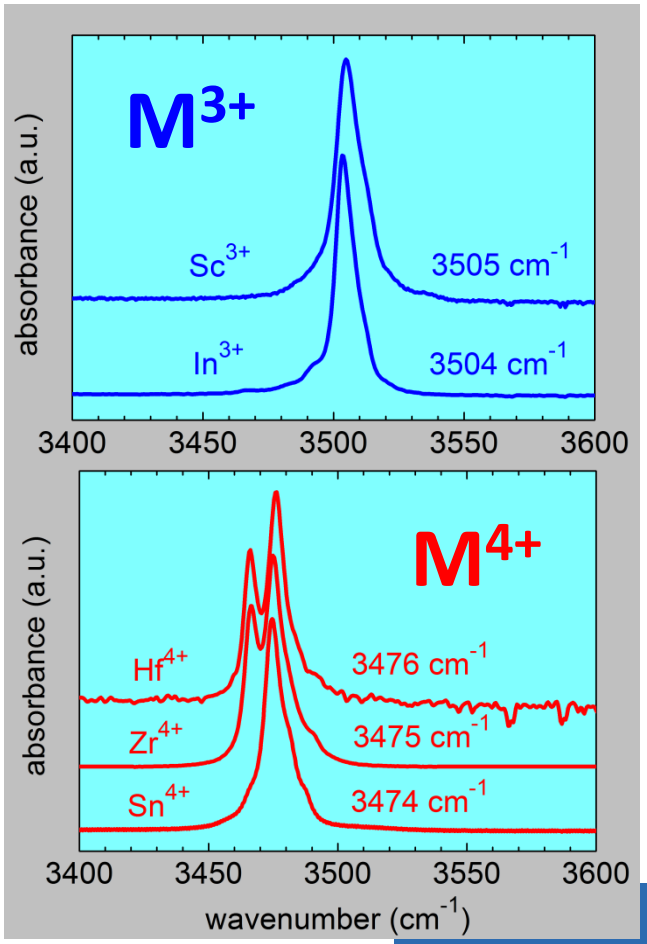

L. Kovács, Zs. Szaller, K. Lengyel, G. Corradi: Hydroxyl ions in stoichiometric $LiNbO_3$ crystals doped with optical damage resistant ions, *Optical Materials*, **37**, 55-58, 2014.

Crystals 2020

i) Hydroxyl ions in ODR ion doped SLN

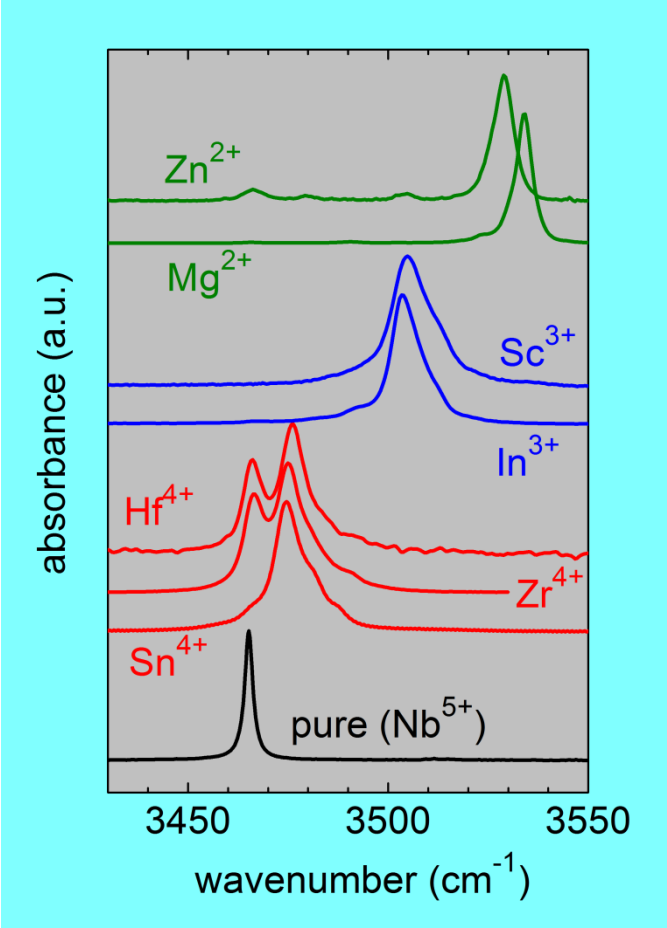

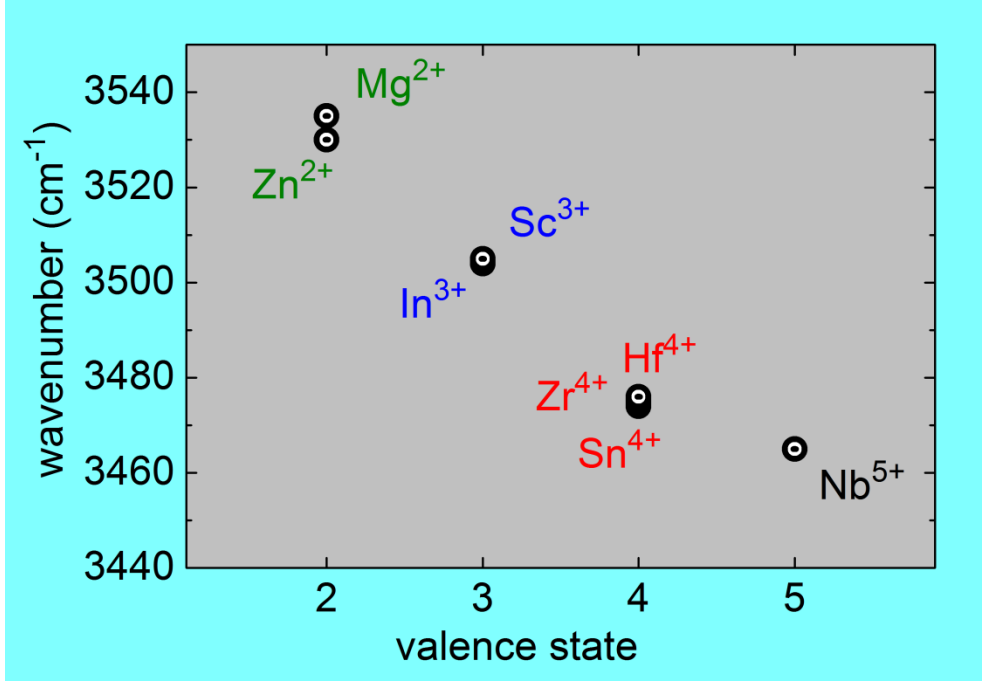

Stronger attractive forces for the protons in M_{Nb}^{2+} - OH^- than in M_{Nb}^{5+} - OH^-

L. Kovács, Zs. Szaller, K. Lengyel, G. Corradi: Hydroxyl ions in stoichiometric $LiNbO_3$ crystals doped with optical damage resistant ions, *Optical Materials*, **37**, 55-58, 2014.

Crystals 2020

i) Hydroxyl ions in ODR ion doped SLN

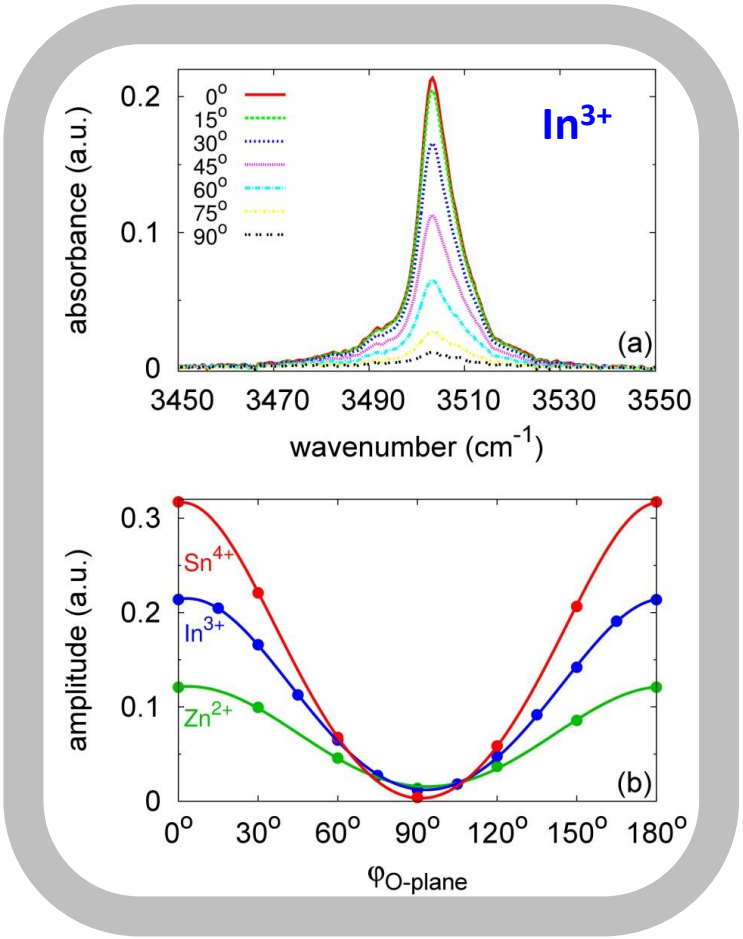

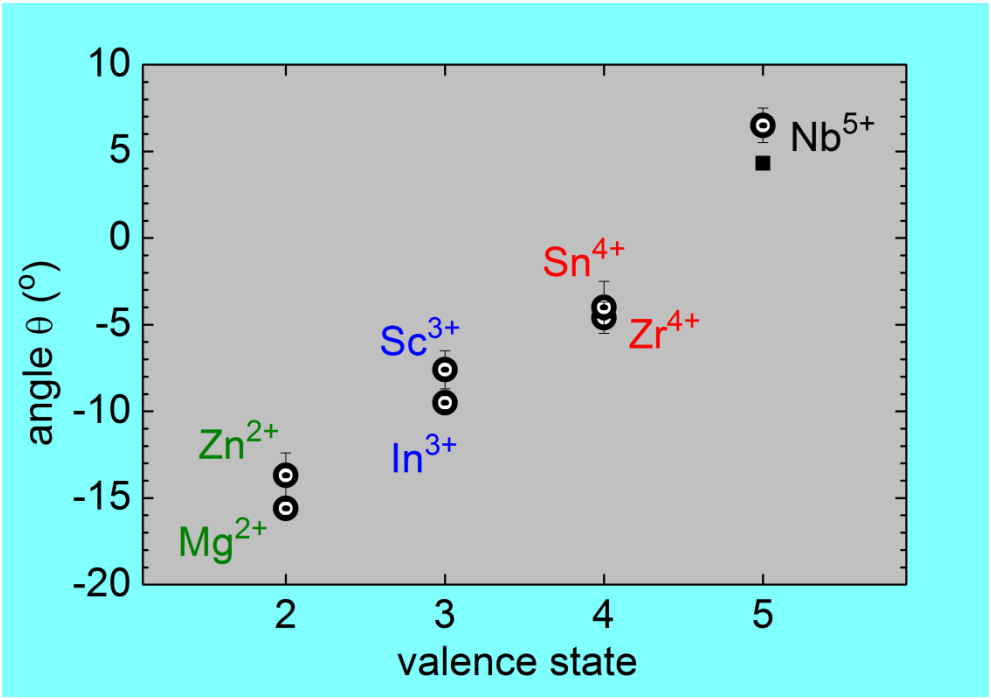

θ is the angle between the O–H bond and the oxygen plane ⊥ to the c axis

L. Kovács, Zs. Szaller, K. Lengyel, G. Corradi: Hydroxyl ions in stoichiometric $LiNbO_3$ crystals doped with optical damage resistant ions, *Optical Materials*, **37**, 55-58, 2014.

Crystals 2020

i) Hydroxyl ions in ODR ion doped SLN

- The new OH^- band is present if $C_{M^{n+}}$ is above the threshold
- OH^- is close to M^{n+}
- Above threshold M^{n+} at least partially occupies Nb site

$$M^{n+}_{Nb} - OH^-$$

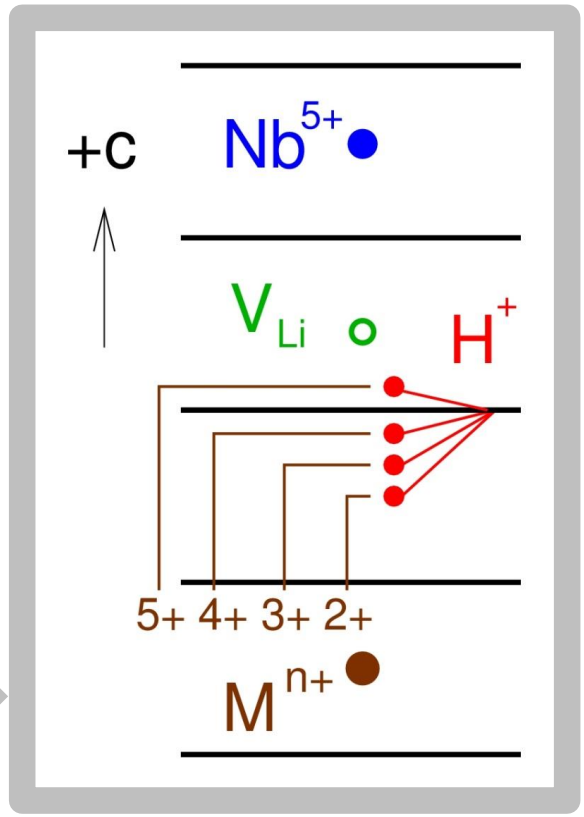

L. Kovács, Zs. Szaller, K. Lengyel, G. Corradi: Hydroxyl ions in stoichiometric $LiNbO_3$ crystals doped with optical damage resistant ions, *Optical Materials*, **37**, 55-58, 2014.

Crystals 2020

i) Dopants in stoichiometric $LiNbO_3$

The defect model

$$M^{n+}_{Nb} - OH^{-}$$

based on the „threshold effect" is valid for all ODR ions.

It should also work for $M^{n+} = RE^{n+}$ and TM^{n+} ions!

Crystals 2020

i) Hydroxyl ions in RE^{3+}-doped SLN

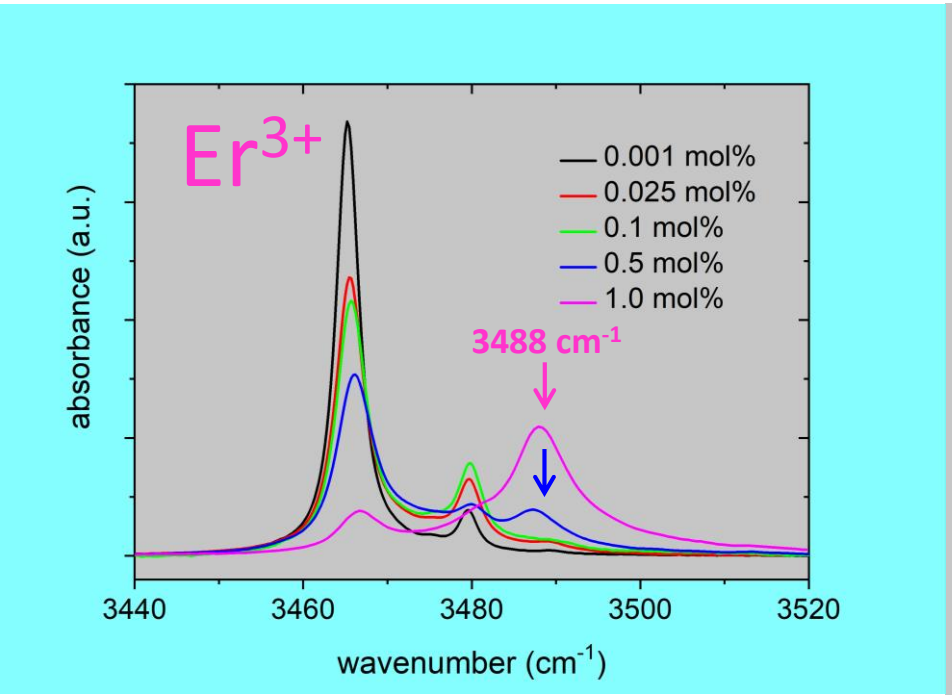

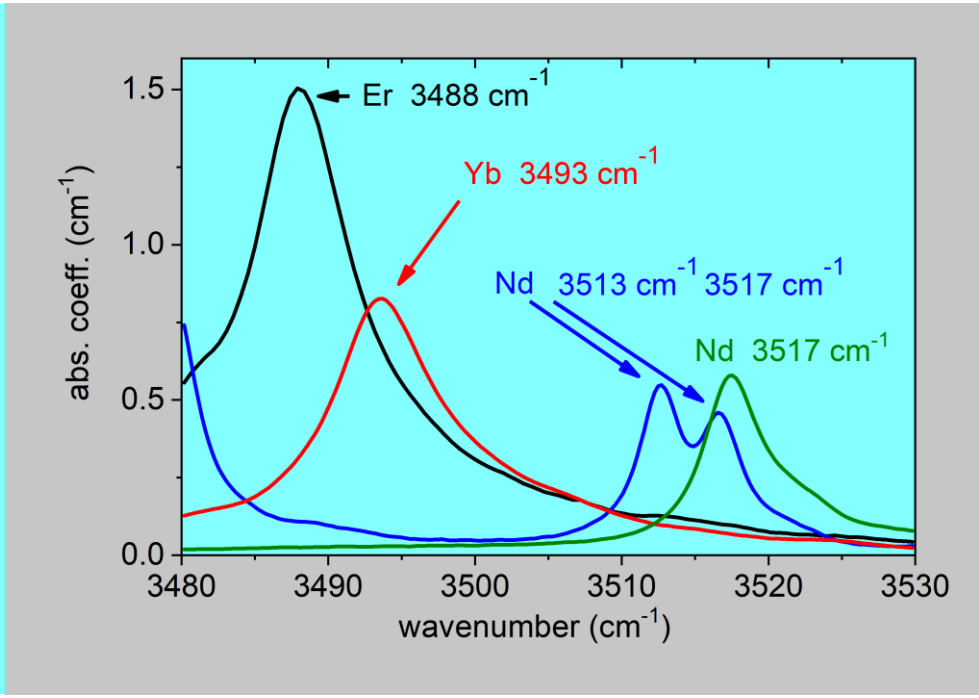

- Above a threshold Er concentration a new OH^- band appears at ≈3488 cm^{-1}
- New OH^- bands appear for other RE^{3+} ions as well

L. Kovács, L. Kocsor, Zs. Szaller, I. Hajdara, G. Dravecz, K. Lengyel, G. Corradi: Lattice site of rare-earth ions in stoichiometric lithium niobate probed by OH^- vibrational spectroscopy, *Crystals*, **7**, 230/1-9, 2017.

Crystals 2020

i) RE^{3+} ions in stoichiometric $LiNbO_3$

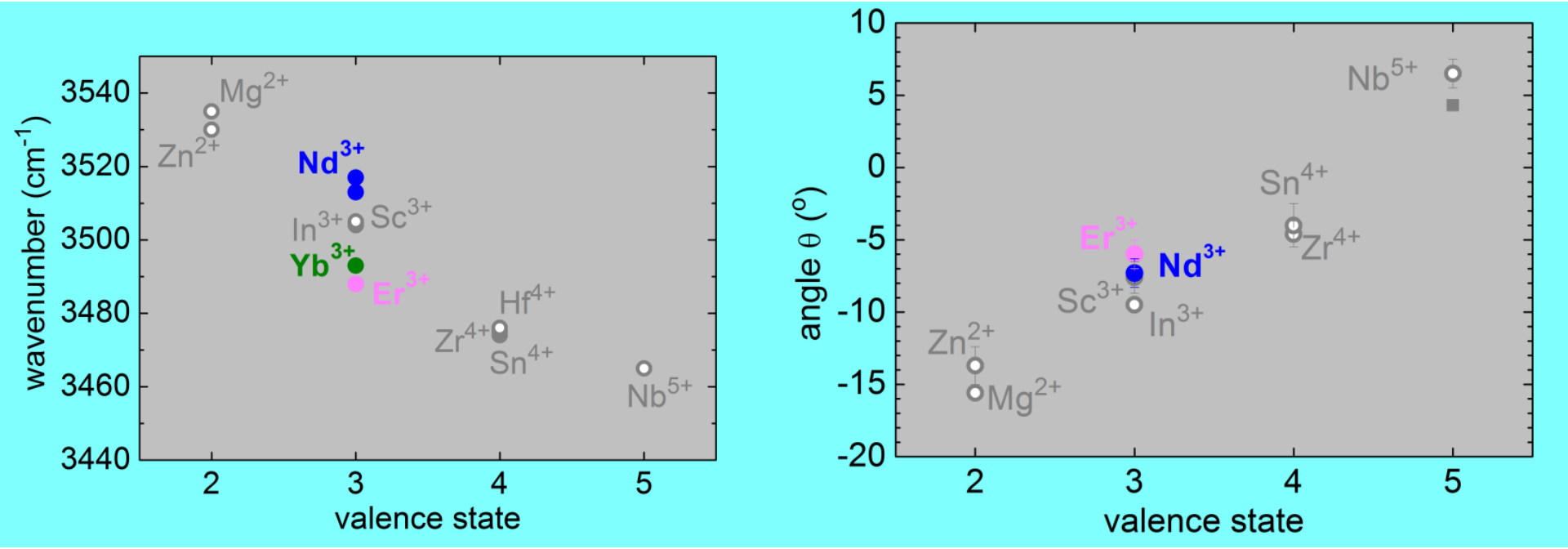

- RE^{3+} ions fit into the incorporation model of ODR ions

L. Kovács, L. Kocsor, Zs. Szaller, I. Hajdara, G. Dravecz, K. Lengyel, G. Corradi: Lattice site of rare-earth ions in stoichiometric lithium niobate probed by OH^- vibrational spectroscopy, *Crystals*, **7**, 230/1-9, 2017.

Crystals 2020

i) TM^{n+} ions in stoichiometric $LiNbO_3$

Ti^{4+}, Fe^{3+}, Fe^{3+}+Ti^{4+} and Cr^{3+} doped SLN crystals were grown by the HTTSSG and Czochralski methods

SLN – HTTSSG
0.12 mol% Ti

SLN – HTTSSG
0.12 mol% Fe

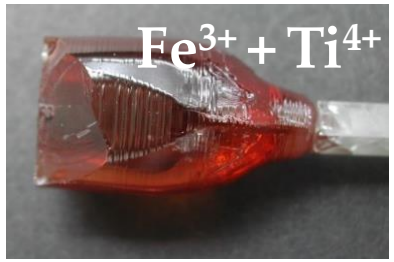

SLN – HTTSSG
0.24 mol% Fe + 0.12 mol% Ti

SLN – HTTSSG
0.5 mol% Cr

SLN – Czochralski
0.5 mol% Cr
Li/Nb=1.38

Sample series	Conc. in solution [mol%]		Conc. in crystal [mol%]		OH^- band [cm^{-1}]	
	Fe	Ti	Fe	Ti	Fe	Ti
1	0.06	0	-	-	-.	-
	0.12	0	0.056	-	-	-
	0.5	0	0.23	-	**3502**	-
2	0	0.012	-	-	-	-
	0	0.06	-	-	-	-
	0	**0.12**	-	0.077	-	**3485**
3	0.012	0.012	-	-	-	-
	0.06	0.06	-	-	-	**3485w**
	0.12	**0.12**	0.068	0.069	**3502vw**	**3485**
	0.24	**0.12**	0.13	0.048	**3502w**	**3485**

Sample series	Growth method	Cr conc. in solution/melt [mol%]	Cr–OH band [cm^{-1}]
4	HTTSSG	0.1	-
	HTTSSG	0.5	-
	Czochralski	0.5	**3502**

L. Kovács, L. Kocsor, É. Tichy-Rács, K. Lengyel, L. Bencs, and G. Corradi: Hydroxyl ion probing transition metal dopants occupying Nb sites in stoichiometric $LiNbO_3$, *Optical Materials Express*, **9**, 4506-4516, 2019.

Crystals 2020

i) OH^- ions in Fe^{3+}- and Ti^{4+}-doped SLN

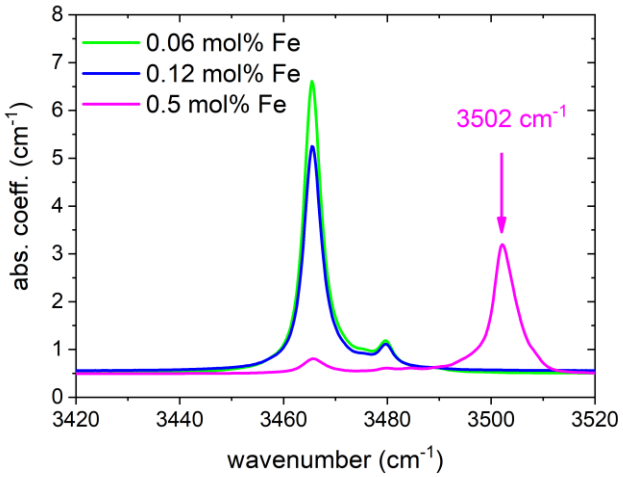

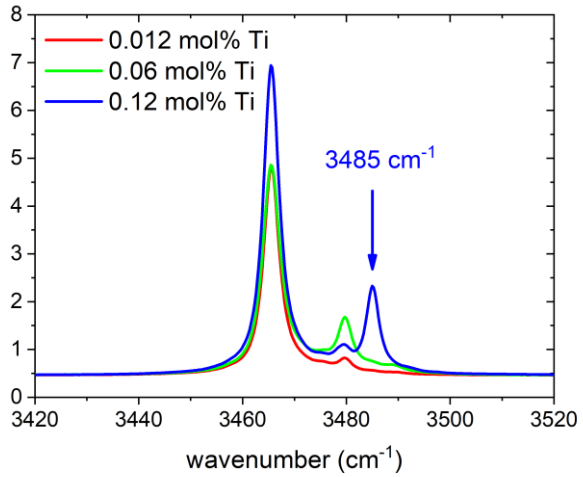

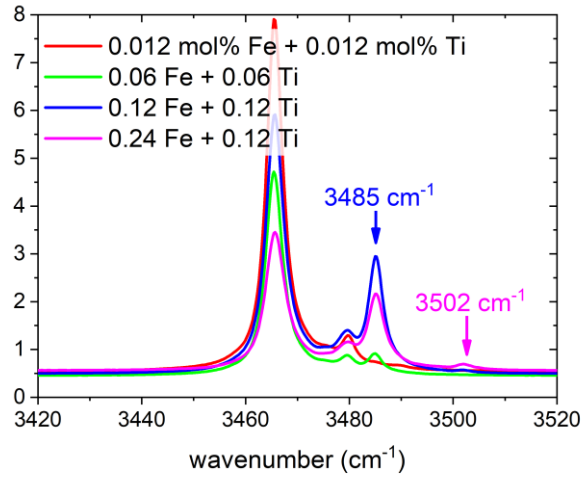

- Above a threshold concentration of the TM^{n+} dopants **new OH^- absorption bands** appear in SLN crystals

L. Kovács, L. Kocsor, É. Tichy-Rács, K. Lengyel, L. Bencs, and G. Corradi: Hydroxyl ion probing transition metal dopants occupying Nb sites in stoichiometric $LiNbO_3$, *Optical Materials Express*, **9**, 4506-4516, 2019.

Crystals 2020

i) Hydroxyl ions in Cr^{3+}-doped SLN

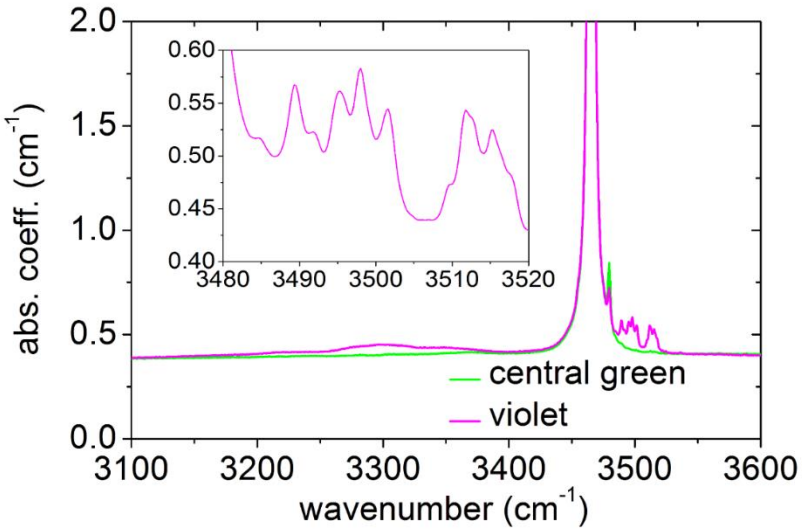

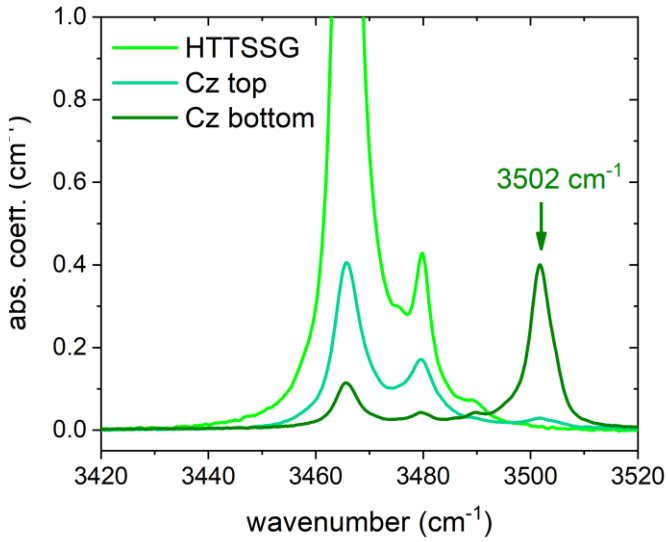

- In the inhomogeneous bottom part of Cr-doped SLN a number of narrow overlapping OH^- bands appeared due to Cr – OH centres with different defect environments

- Due to the composition change (becoming more stoichiometric) a single OH^- band appears at 3502 cm^{-1} at the bottom part of the Czochralski-grown crystal similarly to the Fe-doped SLN

Crystals 2020

L. Kovács, L. Kocsor, É. Tichy-Rács, K. Lengyel, L. Bencs, and G. Corradi: Hydroxyl ion probing transition metal dopants occupying Nb sites in stoichiometric $LiNbO_3$, *Optical Materials Express*, **9**, 4506-4516, 2019.

i) TM^{n+} ions in stoichiometric $LiNbO_3$

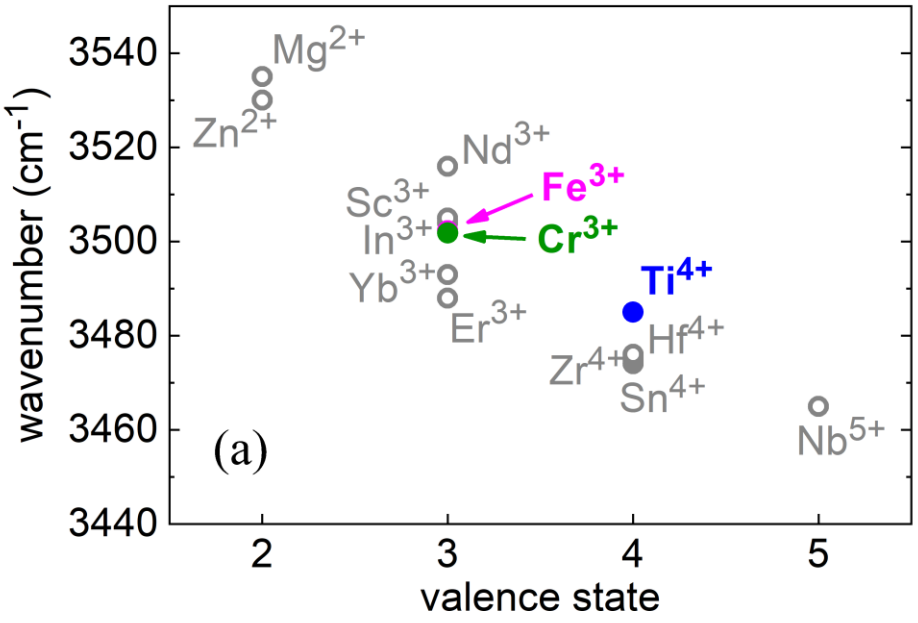

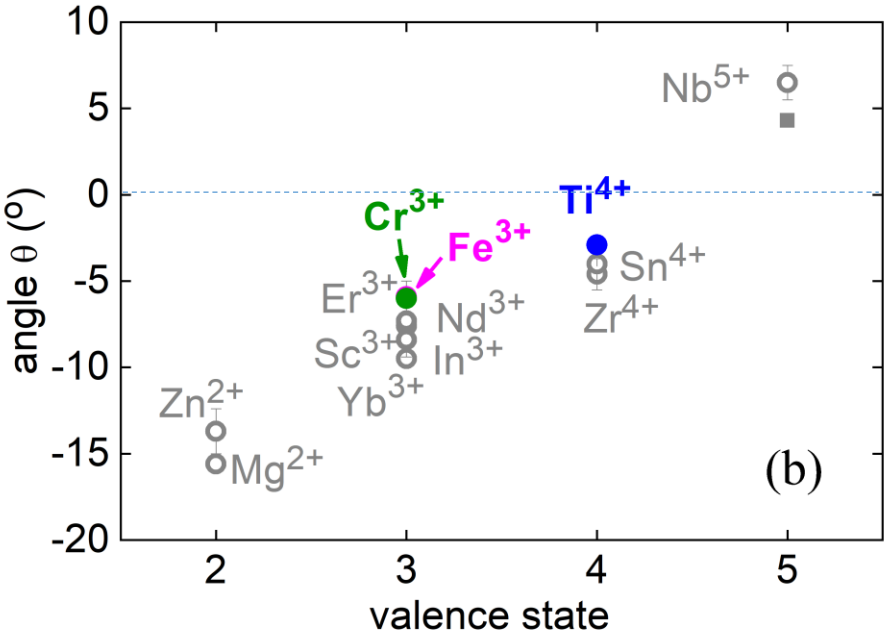

- The higher the valence state of the dopant, the lower the OH^- vibrational frequency and the closer the O–H bond direction to the oxygen plane
- **The observed trend is valid for all dopants studied so far**

L. Kovács, L. Kocsor, É. Tichy-Rács, K. Lengyel, L. Bencs, and G. Corradi: Hydroxyl ion probing transition metal dopants occupying Nb sites in stoichiometric $LiNbO_3$, *Optical Materials Express*, **9**, 4506-4516, 2019.

Crystals 2020

i) M^{n+} ions in $LiNbO_3$ – Summary

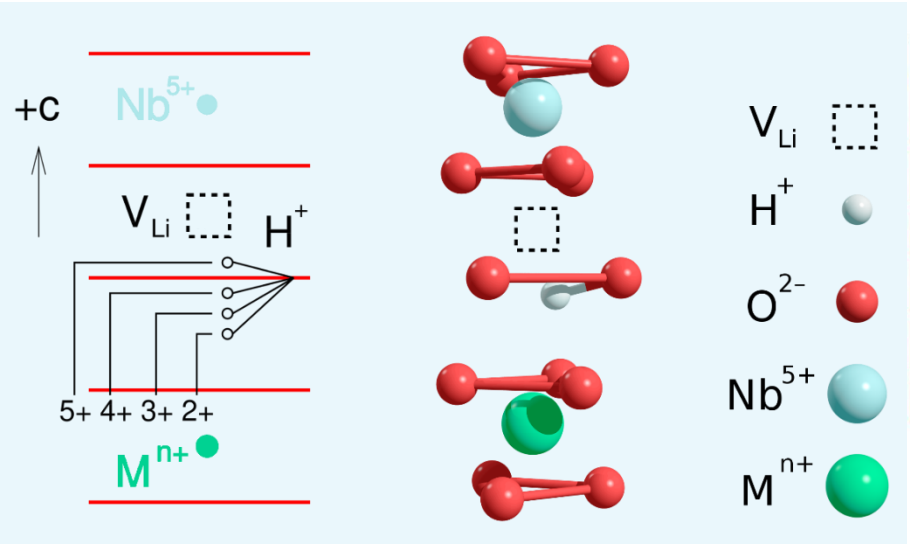

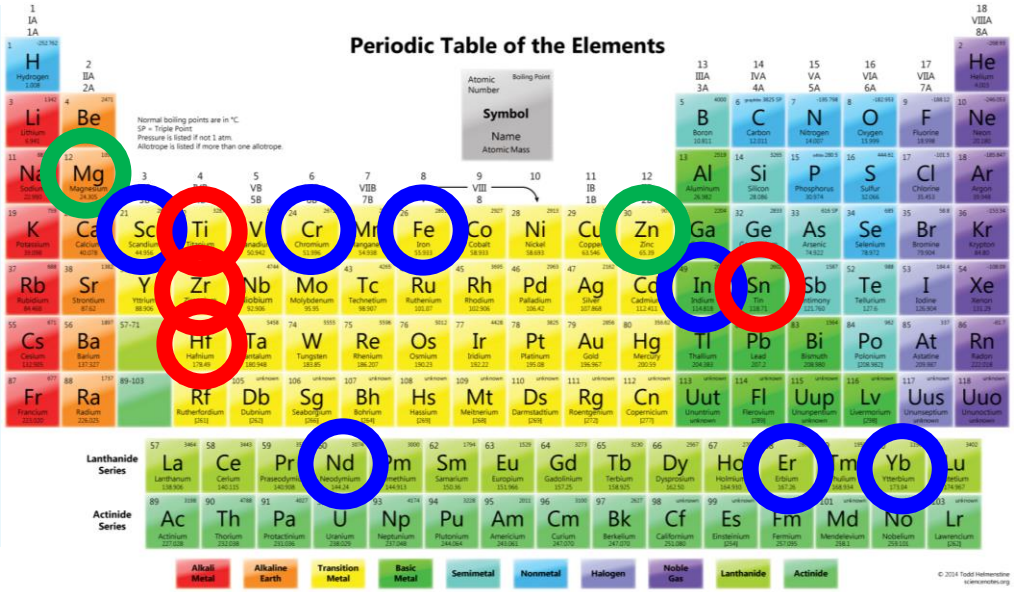

- The IR absorption spectra of the OH^- stretching vibration have been investigated in stoichiometric $LiNbO_3$ doped with M^{n+} (ODR^{n+}, RE^{3+}, TM^{n+}) ions.
- Above a threshold M^{n+} dopant concentration new OH^- absorption bands appear due to the presence of M^{n+}–OH^- type defects in the crystals. In the M^{n+}–OH^- complex the dopant substitutes **Nb** site.
  - **It has been reaffirmed that OH^- ions are excellent probes of the defect structure in $LiNbO_3$ crystals.**

Crystals 2020

ii) Mechanochemical reactions of $LiNbO_3$ induced by high-energy ball-milling

- Lithium niobate nanocrystals
- High-energy ball-milling (dry and wet grinding)
- Particle and grain size reduction
- Phase transformation and chemical reaction
- Structure characterization (X-ray, Raman, reflection spectroscopy, coulometric titration, electron microscopy)

ii) $LiNbO_3$ nanocrystals

- Can be used e.g. in
  - Nonlinear optics – as harmonic nanoparticles (HNP) in nano-biophotonics
  - Quantum optics – rare-earth doped LN as single photon source
- Can be prepared by
  - „Bottom up" method
    - Mechanochemical calcination (grinding + heat treatment)
    - Wet chemical, sol-gel, hydrothermal, combustion, etc.
  - „Top down" method
    - **High-energy ball-milling (dry and wet grinding) for particle and grain size reduction**
      - **Shaker mill – Spex mixer mill**
      - **Planetary mill – Fritsch Pulverisette**
    - Etching

ii) High-energy ball-milling

Dry grinding in SPEX shaker mill

Grinding parameters							
#	Vial	Ball	Time (h)	Number of balls	Ball-to-powder mass ratio	Ball-to-powder volume ratio	Sample quantity (g)
SS-5	Stainless steel	11 mm 5.5 g	5	2	3.8 : 1	2.2 : 1	2.9
ALO-5	Alumina	12.5 mm 4.2 g	5	2	3.8 : 1	4.4 : 1	2.2
ALO-20			20				
TC-5	Tungsten carbide	11 mm 10.7 g	5	2	3.8 : 1	1.2 : 1	5.65

L. Kocsor, L. Péter, G. Corradi, Z. Kis, J. Gubicza and L. Kovács: Mechanochemical reactions of lithium niobate induced by high energy ball-milling, *Crystals*, **9**, 334/1-14, 2019.

ii) High-energy ball-milling

Dry grinding in SPEX shaker mill

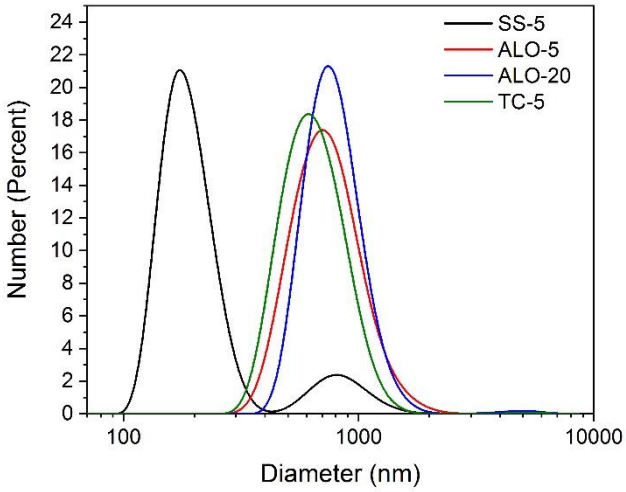

Particle diameter distributions of the ground samples in different vials determined by the Dynamic Light Scattering (DLS) method

#	Resulting particle diameter (nm) DLS	Resulting grain diameter (nm) XRD
SS-5	190, (800)	55±18
ALO-5	700	63±21
ALO-20	700	37±2
TC-5	500	51±6

Particle and grain sizes of samples ground in different vials

L. Kocsor, L. Péter, G. Corradi, Z. Kis, J. Gubicza and L. Kovács: Mechanochemical reactions of lithium niobate induced by high energy ball-milling, *Crystals*, **9**, 334/1-14, 2019.

ii) High-energy ball-milling

Dry grinding in SPEX shaker mill

Sample coloration

- **Al** was detected in the sample ground in **alumina** vial
- No **Fe** and **W** were detected in samples ground in **stainless steel** and **tungsten carbide** vials, respectively
- **The coloration is not related to contamination**

Energy-dispersive X-ray spectroscopy

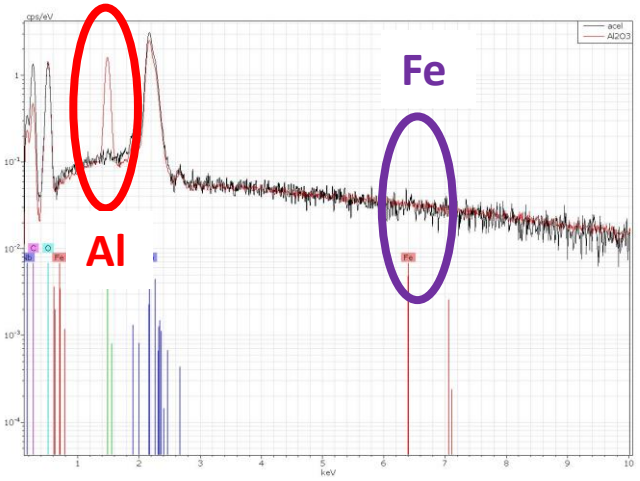

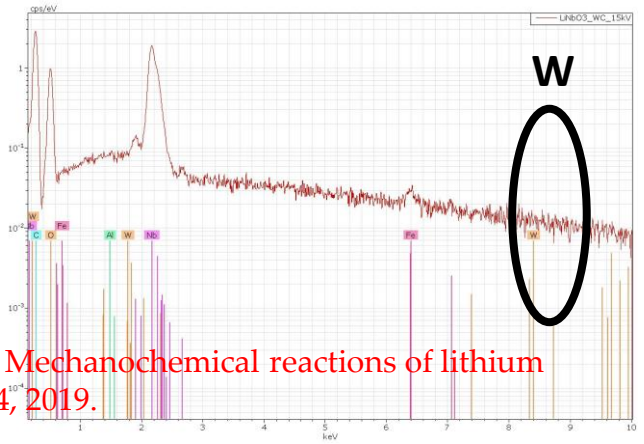

L. Kocsor, L. Péter, G. Corradi, Z. Kis, J. Gubicza and L. Kovács: Mechanochemical reactions of lithium niobate induced by high energy ball-milling, *Crystals*, **9**, 334/1-14, 2019.

Crystals 2020

ii) High-energy ball-milling

Dry grinding in SPEX shaker mill

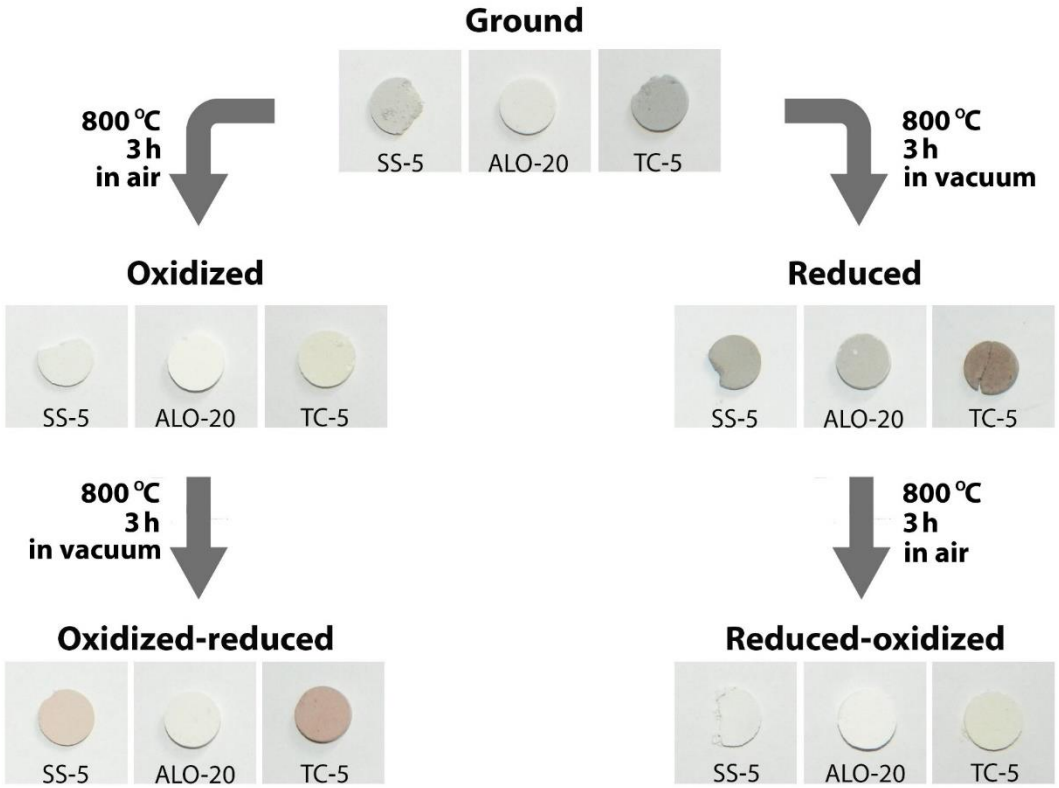

The series of samples ground in different vials with subsequent heat treatments

The samples underwent a change concerning the oxidation state of niobium during the grinding process.
Annealing treatments in oxidative or non-oxidative atmospheres was applied for restoring or modifying the oxidation state of niobium in the ground samples.

L. Kocsor, L. Péter, G. Corradi, Z. Kis, J. Gubicza and L. Kovács: Mechanochemical reactions of lithium niobate induced by high energy ball-milling, *Crystals*, **9**, 334/1-14, 2019.

Crystals 2020

ii) High-energy ball-milling

Dry grinding in SPEX shaker mill

X-ray diffraction

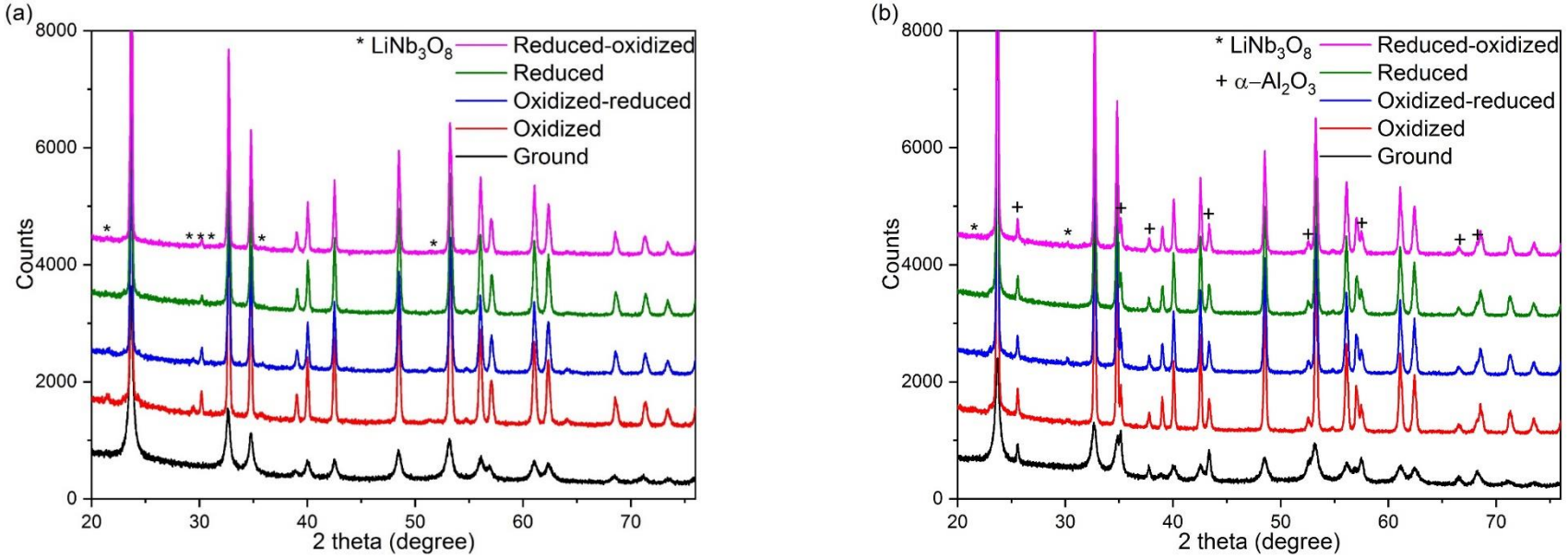

Diffraction patterns of LN ground in **stainless steel** (a) and **alumina** (b) vials
The unmarked peaks are the reflections of $LiNbO_3$

- As-ground samples – broad peaks – small grain size
- Heat-treatment results in narrower diffraction lines due to increased grain sizes
- $LiNb_3O_8$ phase appeared in annealed samples

$$3\ LiNbO_3 = LiNb_3O_8 + Li_2O$$

L. Kocsor, L. Péter, G. Corradi, Z. Kis, J. Gubicza and L. Kovács: Mechanochemical reactions of lithium niobate induced by high energy ball-milling, *Crystals*, **9**, 334/1-14, 2019.

Crystals 2020

ii) High-energy ball-milling

Dry grinding in SPEX shaker mill

Raman spectroscopy

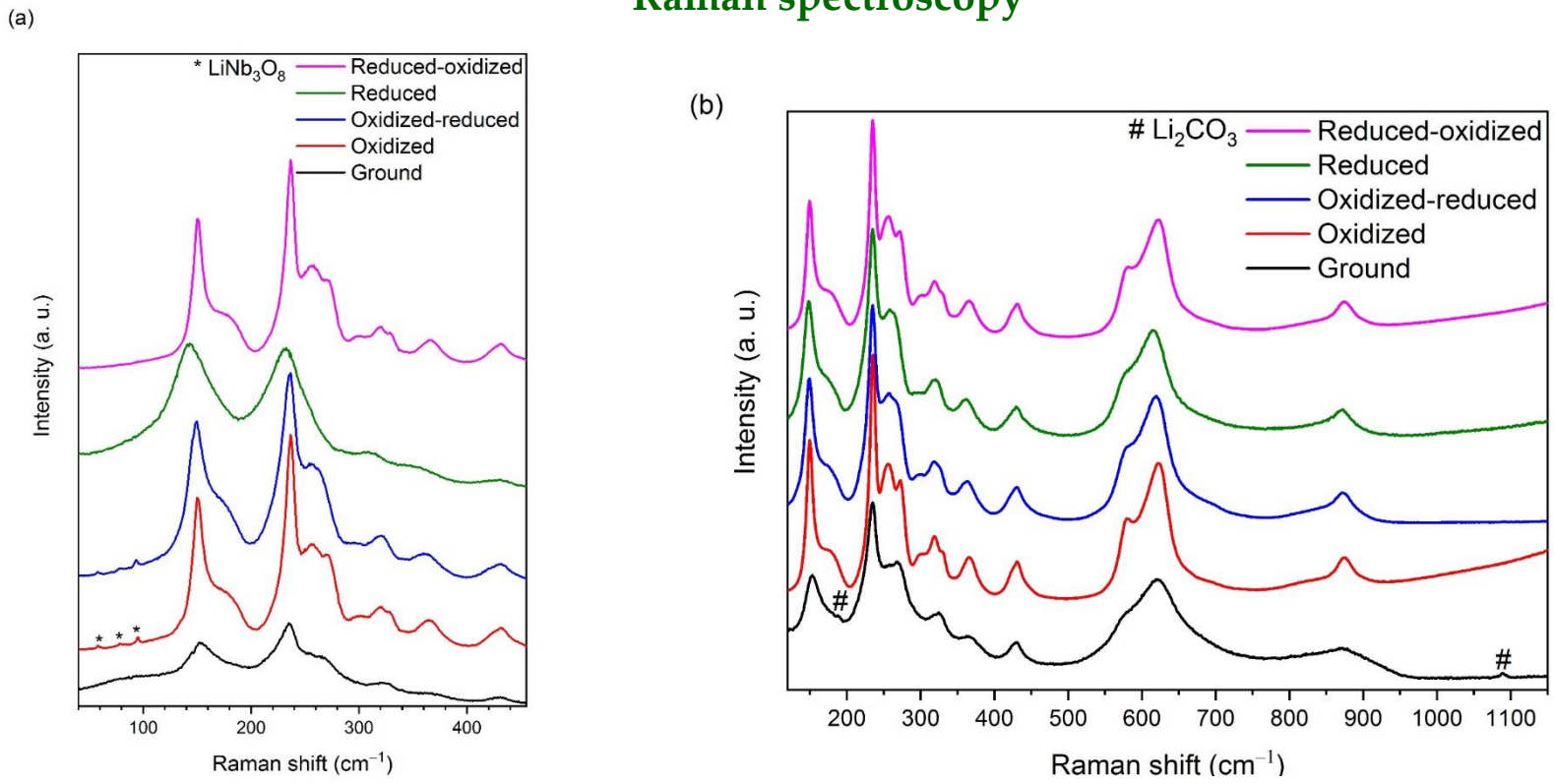

Raman spectra of ground and heat-treated samples ball-milled for 5 h in **stainless steel** (a), and in **tungsten carbide** vial (b)

L. Kocsor, L. Péter, G. Corradi, Z. Kis, J. Gubicza and L. Kovács: Mechanochemical reactions of lithium niobate induced by high energy ball-milling, *Crystals*, **9**, 334/1-14, 2019.

Crystals 2020

ii) High-energy ball-milling

Dry grinding in SPEX shaker mill

Optical reflection measurements

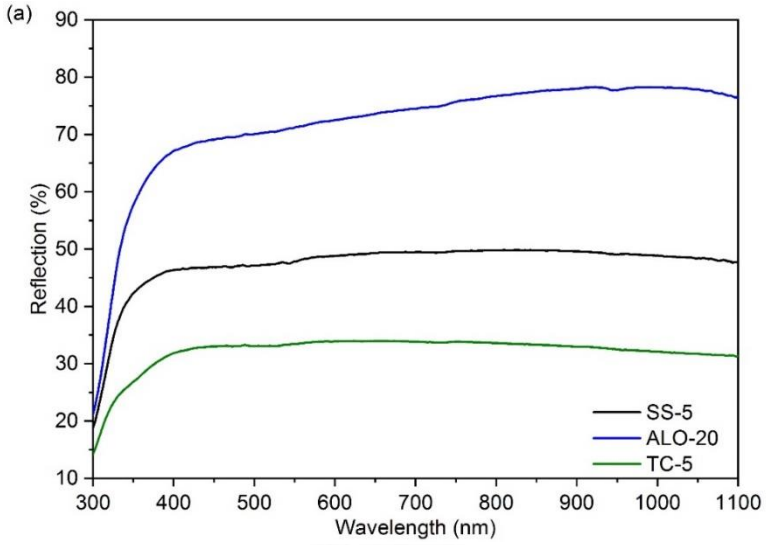

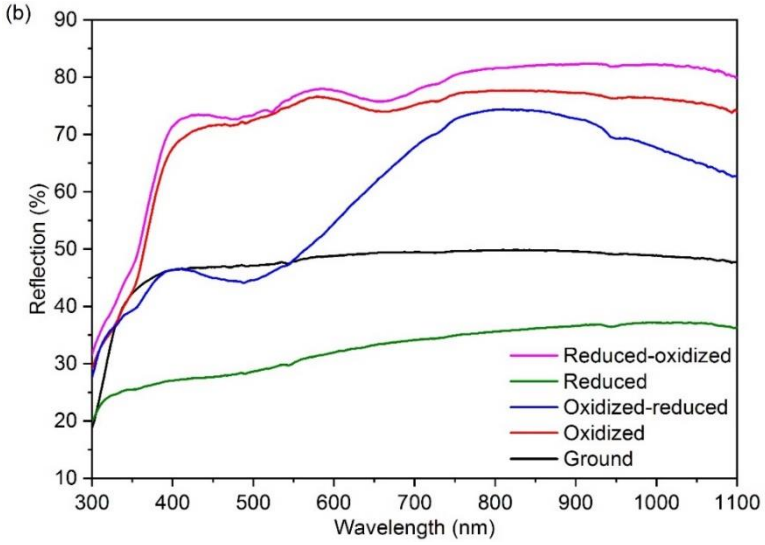

ground ox ox-red red red-ox

Optical reflection spectra of samples ball-milled in different vials (a) and of ground and heat-treated samples ball-milled in **stainless steel** vial (b)

L. Kocsor, L. Péter, G. Corradi, Z. Kis, J. Gubicza and L. Kovács: Mechanochemical reactions of lithium niobate induced by high energy ball-milling, *Crystals*, **9**, 334/1-14, 2019.

Crystals 2020

ii) High-energy ball-milling

Dry grinding in SPEX shaker mill

- Congruent $LiNbO_3$ crystals:
  - $Li_{1-5x}Nb_{1+x}O_3$, x≈0.01
  - Nb_{Li}^{4+} : small polaron
  - Nb_{Li}^{4+} - Nb_{Nb}^{4+} : bipolaron

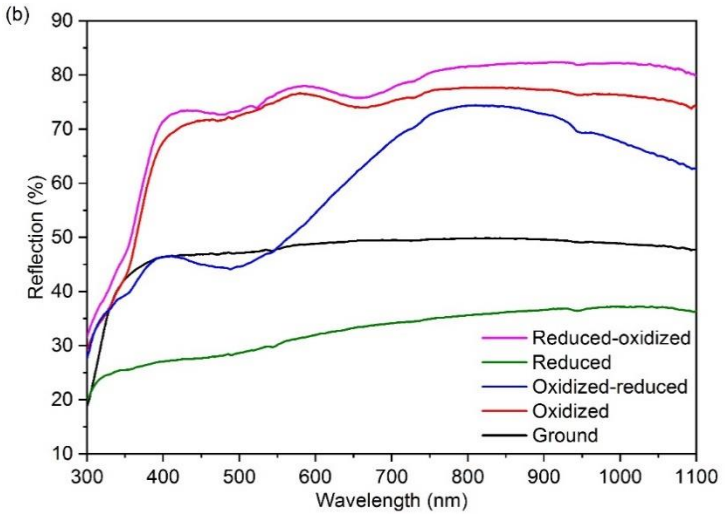

- Ball-milling

$$2LiNbO_3 \rightarrow Nb_{Nb}^{4+} + Nb_{Li}^{4+} + 3O_O^{2-} + 2e^- + Li_2O\uparrow + O_2\uparrow$$

- Oxidation

$$LiNbO_3 + Nb_{Nb}^{4+} + Nb_{Li}^{4+} + 3O_O^{2-} + 2e^- + O_2 \rightarrow LiNb_3O_8$$

L. Kocsor, L. Péter, G. Corradi, Z. Kis, J. Gubicza and L. Kovács: Mechanochemical reactions of lithium niobate induced by high energy ball-milling, *Crystals*, **9**, 334/1-14, 2019.

Crystals 2020

ii) High-energy ball-milling

Dry grinding in SPEX shaker mill

Quantitative determination of the degree of decomposition during ball-milling

- Coulometric titration $m_{OX} = MQ/2F$

  M: molar weight of Li_2O

  Q: charge passed until the equivalence point

  F: Faraday-constant (96485 C/mol)

  2: the hydrolysis of 1 mol of Li_2O results in 2 mols of hydroxide ions

Sample	$100w_{ox}$ (weight%)	Mean particle radius, DLS (nm)
ALO-20	0.97±0.05	350
TC-5	1.05±0.10	250
SS-5	1.52±0.21	95

The measured Li_2O mass ratios w_{ox}, expressed as weight percent of the as-ground powder

L. Kocsor, L. Péter, G. Corradi, Z. Kis, J. Gubicza and L. Kovács: Mechanochemical reactions of lithium niobate induced by high energy ball-milling, *Crystals*, **9**, 334/1-14, 2019.

ii) High-energy ball-milling

Dry grinding in SPEX shaker mill

Estimation of the thickness of the $LiNb_3O_8$ layer

- Assumptions
  - Uniform spherical LN particles of unmodified composition
  - Uniformly thick $LiNb_3O_8$ layer
  - $d \ll R$

$$w_{OX} = \frac{m_{LTN}\frac{M_{OX}}{M_{LTN}}}{m_{LN}+m_{LTN}\left(1+\frac{M_{OX}}{M_{LTN}}\right)},$$ weight ratio of Li_2O in the ground material

$$d_{LTN} \approx \frac{R}{3}\frac{\rho_{LN}}{\rho_{LTN}}\frac{M_{LTN}}{M_{OX}}w_{OX} \text{ and } d_{OX} \approx \frac{\rho_{LTN}}{\rho_{OX}}\frac{M_{OX}}{M_{LTN}}d_{LTN} \approx \frac{d_{LTN}}{5.6}$$

Sample	$100w_{ox}$ (weight%)	Mean particle radius, DLS (nm)	Mean grain radius, XRD (nm)	d_{LTN} $LiNb_3O_8$ shell thickness (nm)	d_{OX} Li_2O shell thickness (nm)
ALO-20	0.97±0.05	350	18.5	14.6	2.6
TC-5	1.05±0.10	250	25.5	11.3	2.0
SS-5	1.52±0.21	95	27.5	6.2	1.1

L. Kocsor, L. Péter, G. Corradi, Z. Kis, J. Gubicza and L. Kovács: Mechanochemical reactions of lithium niobate induced by high energy ball-milling, *Crystals*, **9**, 334/1-14, 2019.

Crystals 2020

ii) High-energy ball-milling

Dry and wet grinding in Fritsch planetary mill

Recent results

Grinding parameters						
	Vial / Ball	**RPM**	**Time**	**Solvent**	**Ball size / quantity**	**Sample quantity**
DRY	ZrO_2	1100	10x1 min	-	0.5-3 mm / 70 g	5 g
WET	ZrO_2	1100	10x1 min	10 ml water	0.1-3 mm / 70 g	5 g

ii) High-energy ball-milling

Dry and wet grinding in Fritsch planetary mill

Recent results

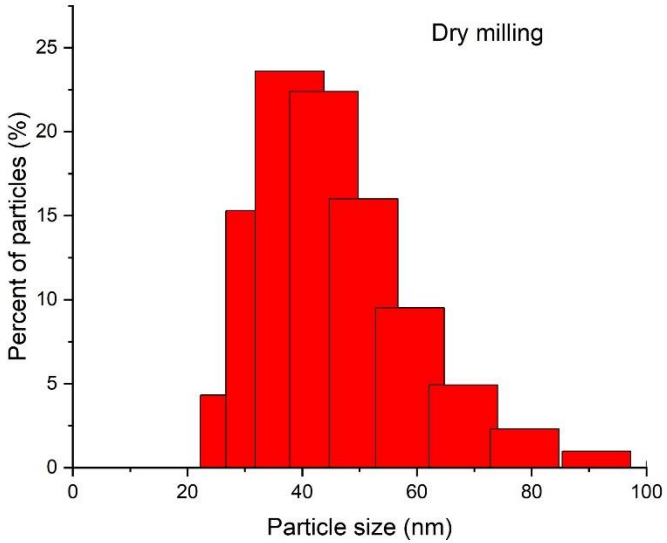

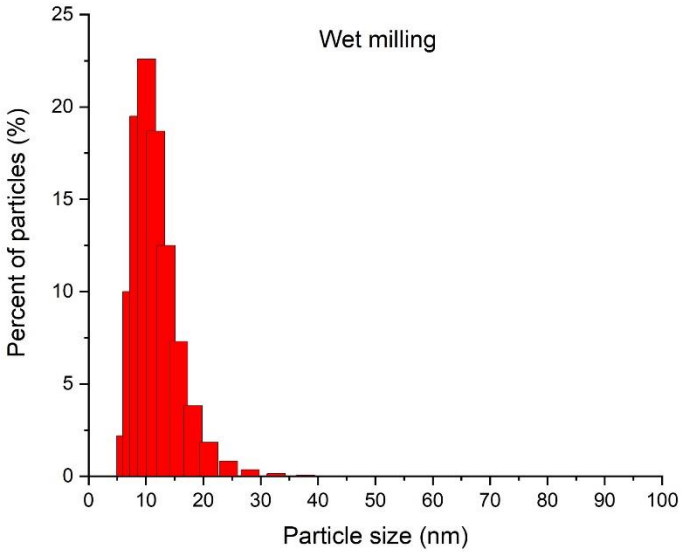

Size distribution measured by Dynamic Light Scattering (DLS)

Crystals 2020

ii) High-energy ball-milling

Dry grinding in Fritsch planetary mill

Recent results

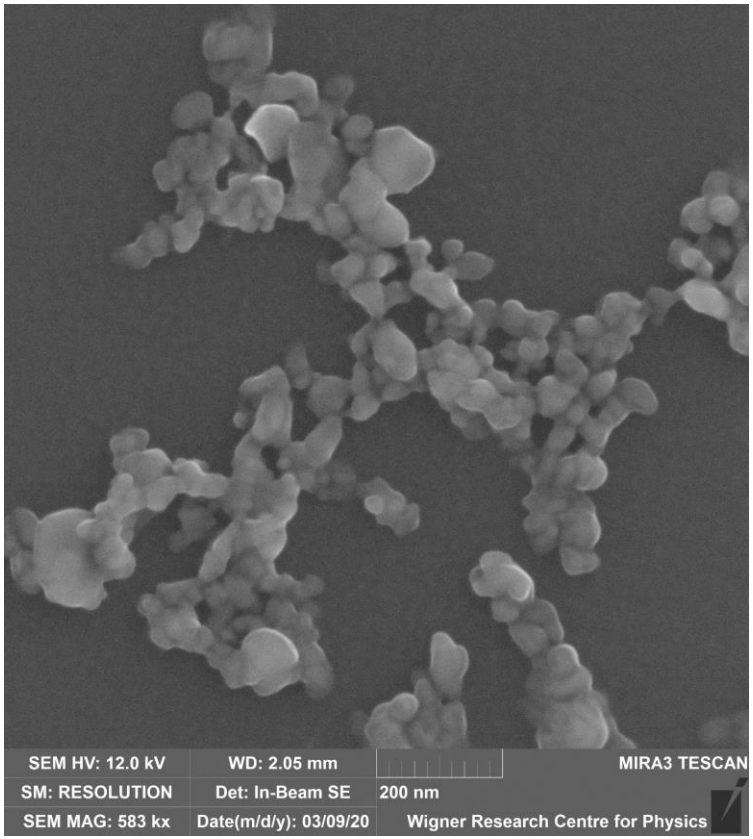

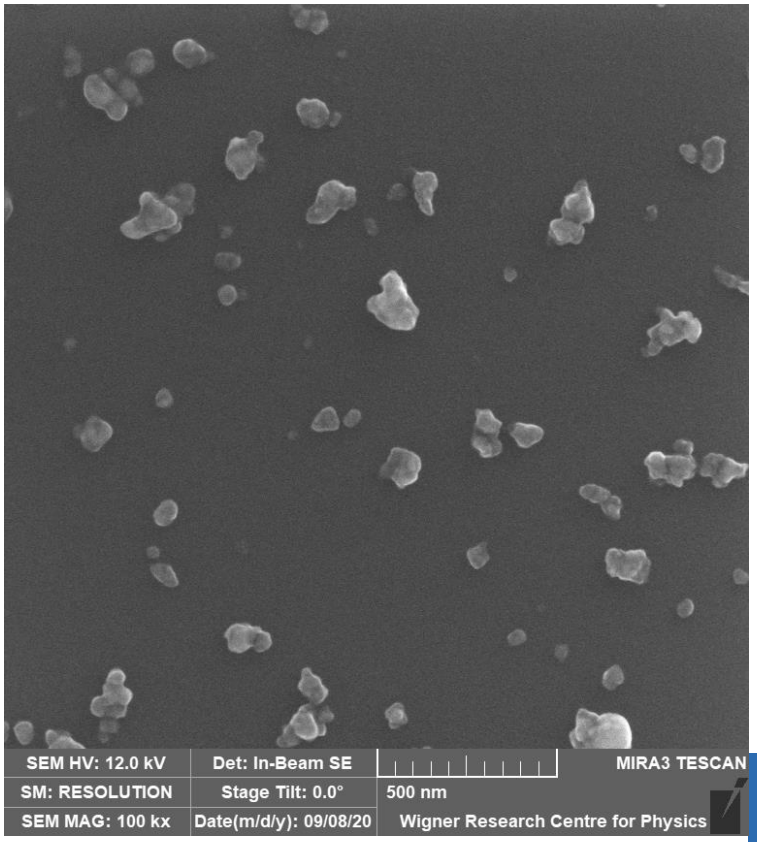

Scanning electron microscopy (SEM) images of the $LiNbO_3$ particles

Crystals 2020

ii) High-energy ball-milling

Wet grinding in Fritsch planetary mill

Recent results

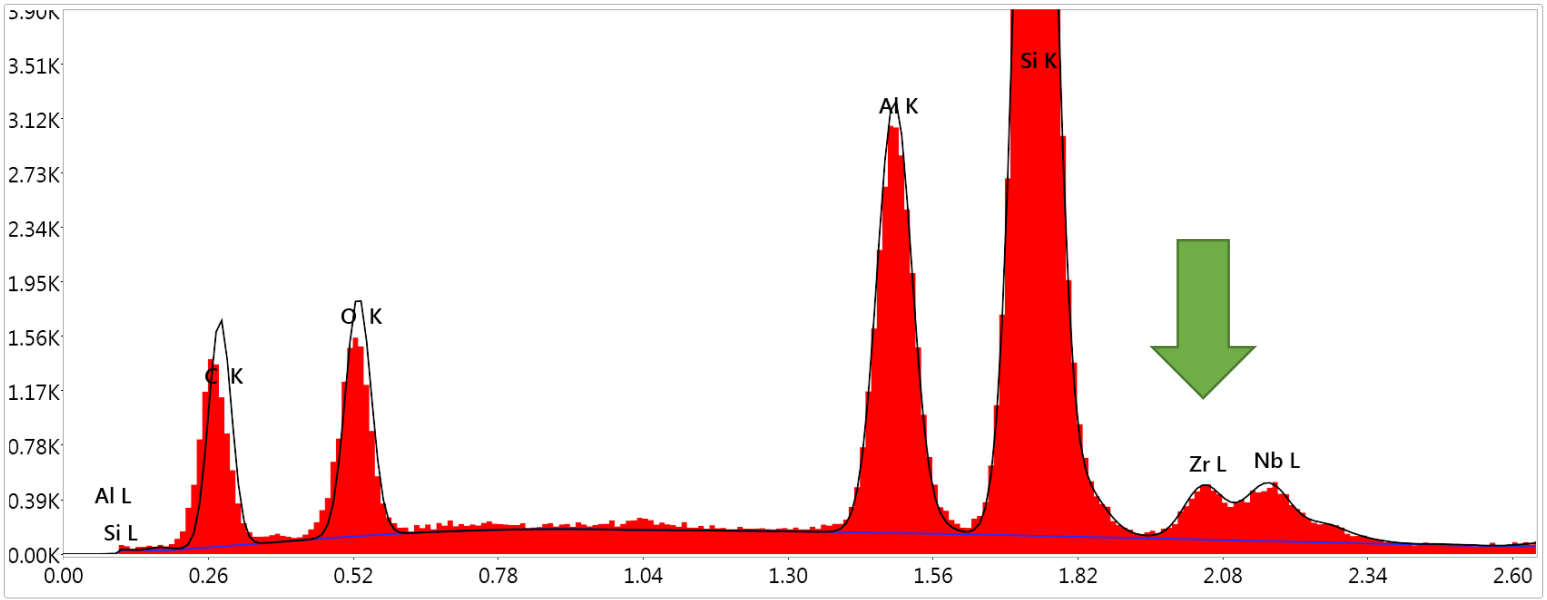

The material (Zr) of the vial/ball is present in the particles measured by EDAX

Crystals 2020

ii) High-energy ball-milling

Dry grinding in Fritsch planetary mill

Recent results

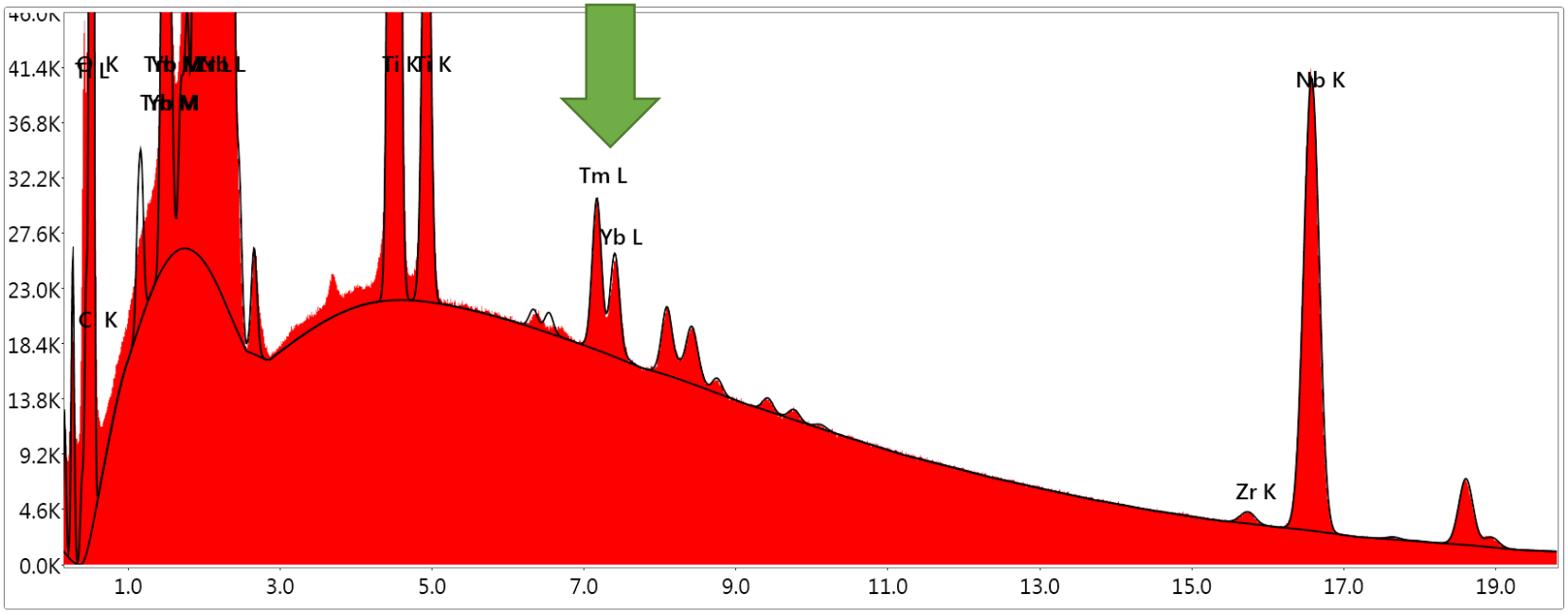

Dopants (Tm and Yb) planned to use in single photon source are present in the particles

Crystals 2020

ii) High-energy ball-milling – Summary

- Nano-LN (10-50 nm particle size) has been successfully prepared by high-energy ball-milling
- During the milling process the material suffers partial reduction interpreted by polaron/bipolaron formation.
- Li_2O loss and $LiNb_3O_8$ formation was observed in the outer shell of the particles
- These findings provide a comprehensive explanation of the physicochemical behaviour of the system during grinding and annealings.
- **RE^{3+}-doped nano-LN has been successfully prepared for single photon source**

Crystals 2020

Conclusions

- **$LiNbO_3$ either in single crystal or in nanocrystalline form is one of the most versatile materials for optical applications**

- **The study of both intrinsic and extrinsic defects affecting the properties of LN may provide new results for future applications**

Crystals
2020

Acknowledgment

Crystals 2020